Origin of Co-Conformational Selectivity in a [3]rotaxane

Xiange Zheng and Karl Sohlberg*

Department of Chemistry, Drexel University, 3201 Chestnut Street, Philadelphia, Pennsylvania 19104

Received: November 17, 2005; In Final Form: August 22, 2006

Co-conformational selectivity and structure−energy relationships in a [3]rotaxane are investigated with a recently developed multiple-sampling and statistical analysis procedure for modeling interlocked molecules and mechanical molecular devices. The results presented confirm the experimentally observed co-conformational selectivity. The theoretical calculations reveal that ring−ring interactions are very small and ring−shaft intercomponent interactions decide the co-conformational preference. In particular, it is found that stronger ring binding at the central binding station on the shaft than at either of the two terminal binding stations gives rise to the observed co-conformational preference. Analysis of radius of gyration data shows that co-conformational isomerism is not strongly correlated to coiling of the shaft.

1. Introduction

As the drive to miniaturize mechanical devices approaches the nanometer scale, mechanically interlocked molecules, such as rotaxanes,[1−8] catenanes,[3,6−17] and knots[18]are currently attracting considerable interest. A rotaxane is a molecular complex consisting of two types of components; a long dumbbell-shaped chain molecule, which is called the shaft, threads one (or more) ring molecule(s), typically a crown ether(s) or cyclodextrin(s). The components are chemically independent but mechanically interlocked so that the complex cannot be dissociated without breaking at least one chemical bond. When such complexes are synthesized so that the number of inter-component binding stations is equal to or greater than the number of components, multiple-stability results. The conceptual step from a multiply stable rotaxane to a functional molecular device would appear to be a small one, hence the current great interest in these systems. For example, Chiu el al.,[19] reported the fabrication of a bistable [3]rotaxane. The [3]rotaxane is comprised of one shaft and two crown components, with three cationic recognition sites located on the shaft for the binding of the two crowns, hence there is a deficiency of rings by design. The complex is therefore topologically equivalent to a single rung on an abacus. Our primary goal is to study the multiple stability of this system and identify the origins of co-conformational selectivity.

Because of their large molecular size, the modeling of such molecular-based devices is a current major challenge to computational chemistry. Only recently have advances in computer hardware and software technology brought molecular device modeling into the realm of possibility. Pioneering modeling studies include work by Leigh et al.[20] reporting the simulation of the rate of circumrotations in a catenane system by reduced-dimensional quantum-mechanical modeling. Deleuze et al.[21] provided a theoretical description of the lowest energy pathway for the circumrotation of macrocycles in a catenane system by using molecular mechanics (MM) calculations to model the molecular potential energy surface (PES) and employing unimolecular reaction rate theory. In another MM-based study, Leigh et al.[22] investigated the factors that affect the rate of macrocyclic ring rotation in benzylic amide [2]-catenanes. Such motions are crucial for switching among different interlocking positions in catenanes. The fundamental basis for the stabilization of molecular complexes was investigated by Raymo et al.[23] employing empirical force field and ab initio quantum mechanical calculations.

Previously, we demonstrated a computational procedure capable of successfully modeling systems of interlocked molecules.[24,25] In this work, the procedure is employed and extended to investigate a multiply stable cationic (+3 charge) [3]rotaxane, one of the most complicated molecular-device systems that has been modeled to date. This system is of larger size and greater topological complexity than any system yet modeled with our multiple-sampling and statistical analysis procedure. Additional complexities not previously modeled include the involvement of two cyclic ring components and three recognition sites on the shaft. To model this system, abbreviated (10-step) geometrical optimizations were performed for a large set of structures. Statistical analysis of the results yields the structure−energy profile. Full optimizations were then carried out for 100 low energy co-conformations to validate the above-generated profile, and to obtain further structural and binding details of the system.

2. Theoretical Methods

2.1. Review of Statistical Sampling Methodology. The functionality of switchable rotaxanes is typically driven by a change in charge or electronic state, necessitating that an explicitly quantum-mechanical electronic structure description be employed in their modeling. In light of their large molecular size, this constraint leads to a significant computational challenge. To meet this challenge we combine efficient semiempirical electronic structure methodology with a multiple-sampling and statistical analysis procedure, the details of which have been presented elsewhere.[24]

In brief, the multiple-sampling and statistical analysis procedure is based on the concept that sampling the molecular potential energy surface (PES) at points *near-to* local minima (stable co-conformations) will produce an approximation to the true density of conformational states (DOCS) function. We assume that the PES (f) in the vicinity of any local minimum

* To whom correspondence should be addressed. E-mail: sohlbergk@drexel.edu.

10.1021/jp056665a CCC: $33.50
Published on Web 10/04/2006

can be adequately expressed by a quadratic expansion in normal coordinates α_i^n,

$$f(\alpha_i^n) \approx c^n + \sum_i [\alpha_i^n - \alpha_i^{\circ n}]^2 \frac{k_i^n}{2} \quad (1)$$

where c^n and k_i^n are constants, and $\alpha_i^{\circ n}$ are the values of coordinates at the true minima. The subscript "*i*" denotes the *i*th coordinate. The superscript *n* denotes the *n*th local minimum. There is a one-to-one correspondence between these local minima and stable co-conformations. Identifying a co-conformation is therefore equivalent to finding all of the $\alpha_i^{\circ n}$ for a particular *n*.

We define *G(f)* to be the sum of conformational states function (i.e., the number of local minima for which the total energy is less than *f*). It follows that

$$G'(f) = \frac{dG(f)}{df} \quad (2)$$

is then the *density of conformational states* function (DOCS). It may be shown[24] that if the values of the coordinates at the minima $\alpha_i^{\circ n}$ are located approximately, the relative error introduced into the DOCS function is linearly proportional to the error in specifying the $\alpha_i^{\circ n}$. It follows that a sample of approximate minima contains qualitatively correct information about the DOCS.

In the present case, we define the "true" PES to mean that given by the AM1 Hamiltonian.[26] (In this statement we ignore the approximate nature of the AM1 Hamiltonian and accept the potential energy surface defined by the AM1 Hamiltonian as the "true" surface.) To find *approximate* minima in this surface, we construct various starting structures from rotaxane components whose structures have been optimized to local minima using an empirical-potential method. We then refine these starting structures by abbreviated optimization (partial optimization) based on the AM1 Hamiltonian. The abbreviated optimizations have the effect of locating approximately the values of $\alpha_i^{\circ n}$. In other words, the $\alpha_i^{\circ n}$ found by abbreviated optimization are in the neighborhood of the true values, i.e., the minima in *f* are located approximately. A set of approximate minima gives an approximate DOCS. Upon full optimization of all structures, the predicted DOCS would converge to the true DOCS. The details of these steps are presented in the subsections to follow.

We use the term "starting structures" for the un-optimized rotaxane structures as constructed from the components. The rotaxane structures after abbreviated structural optimization we refer to as "co-conformations" while recognizing that they are in fact *approximations* to co-conformations (as defined by an approximate molecular Hamiltonian). A small subset of these structures is subjected to full structural optimization, (again at the AM1 level) and we refer to these as "fully optimized co-conformations."

2.2. Structural Fundamentals. The [3]rotaxane consists of one dumbbell-shaped shaft and two identical dibenzo-[24]crown-8 (DB24C8) components. These components are presented in Figure 1. To assist in building and analyzing structures, 13 subdivisions of the shaft are defined. These are termed "segments" and are indexed 1−13 as shown in Figure 1. The shaft contains three $-NH_2^+-$ groups, which serve as binding sites for the two DB24C8 rings. Note that there are two chemically distinct binding sites. The two terminal $-NH_2^+-$ groups possess the same chemical environment, but the chemical environment of the central $-NH_2^+-$ group is unique. This distinction is quite important for understanding the origins of co-conformational selectivity. The three binding sites are indexed as 3, 7, and 11 respectively in Figure 1. Throughout the structural assignment and data analysis, the "nominal ring plane" (nrp) of a ring is defined using three of the four bridge C atoms on the two terminal phenyl rings. The centroid of a ring is defined using the atoms C5−C11 and C16−C22, which tend to be visually close to the ring plane (see Figure 1b).

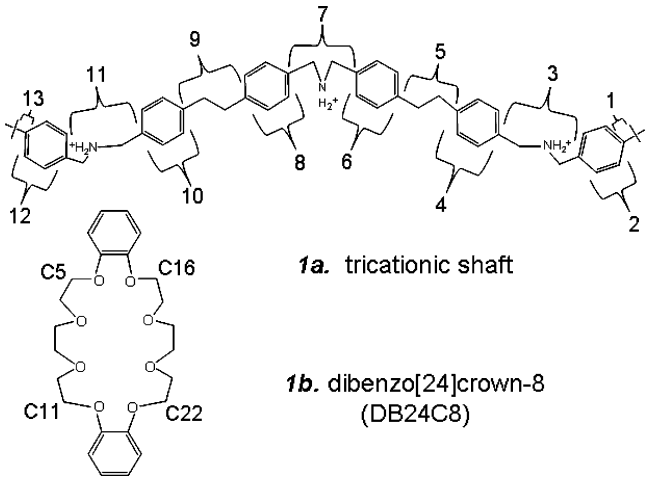

Figure 1. Schematic drawings of the components of the [3]rotaxane complex, which consists of the shaft (**1a**) and two DB24C8 (**1b**) crowns. The shaft is partitioned into 13 segments. For clarity, hydrogen atoms are not shown.

2.3. Subcomponent Conformational Searching. To obtain starting structures for the rotaxane components, full torsional-space conformational searching was performed for the crown and the neutral (unprotonated) shaft components separately, using empirical potential methods, which resulted in 29 crown and 110 shaft conformations, respectively. From the total 29 crown and 110 shaft conformations, two and 16 unique and chemically reasonable ones were selected for construction of the [3]rotaxane complex. Of the 29 crown conformations, two unique ones were selected because only in these conformations was the cavity sufficiently large to accept the shaft. Of the 110 shaft conformations, 16 were selected as being sufficiently unconvoluted to thread two rings. Selections were made by visual inspection using a graphical user interface molecular editor. For each of the 16 shaft conformations, each of the three $-NH-$ groups was protonated to form $-NH_2^+-$ by adding one extra H atom to the sp^3 hybridized N atom, and therefore the shaft component takes on a +3 charge.

2.4. Complex Structure Creation. With the 16 shaft conformers and 2 crown conformers, each choice of shaft conformer was then individually integrated with two crown components in all possible combinations. (The two crowns were allowed to take on the same or different initial conformations.) The two crowns were placed around two different segments of the backbone of the shaft, in an orientation where each of the two chosen segments pierces through the center of its corresponding ring component perpendicular to the nrp of the corresponding ring. Given the equality of the two rings, we consider the first half of the shaft (segments 1−7) for the position of one ring, (the position of the first ring is indexed by n_{b1}), and the whole shaft (segments 1−13) for the position of the other ring (the position of the second ring is indexed by n_{b2}). Considering steric hindrance, the two terminal segments may be ignored, as well as structures with very closely spaced rings. Situations considered here include $n_{b1} = 2-7$, $n_{b2} = 4 \sim 12$ with $n_{b2} > (n_{b1} + 1)$. All possibilities for the two ring

TABLE 1: Possible Locations of the Two Ring Components Indexed by the Segments of the Shaft where the Rings Encircle

choice for n_{b1}[a]	choice for n_{b2}[b]	no. of possibilities[c]
2	4−12	9
3	5−12	8
4	6−12	7
5	7−12	6
6	8−12	5
7	9−12	4
total		39[d]

[a] The location of the first ring component indexed with n_{b1}. [b] The location of the second ring component indexed with n_{b2}. [c] The number of possible locations of the second ring for each specific first-ring position. [d] Total number of possible combinations of locations for the two ring components.

positions are summarized in Table 1. Some redundancy remains when one considers the symmetrical connectivity of the shaft. Next, three possibilities were considered for the orientation of each crown: 0, 60, and 120° (the structure at 180° orientation is roughly equivalent to the one at 0°). Taking into account all the possible combinations of the following parameters: shaft conformations (**16**), the positions of the two rings (the total number is **39** as shown in Table 1), and the conformations (**2**) and orientations (**3**) for each of the two rings, the total number of starting structures for the complex generated through this procedure is 22464 (=16 × 39 × 2 × 2 × 3 × 3).

While the two crown conformers used are chiral because they have no mirror-plane of symmetry, they lack any atomic chiral centers. Consequently, interconversion among various crown configurations is facile owing to the tremendous flexibility of the crown ether backbone.[27,28] Our procedure therefore focuses on generating starting structures that broadly sample the possible positions of the rings relative to the shaft, since a ring can readily convert conformation upon structural relaxation. To demonstrate this assertion, final structures of the crown ether ring components were extracted from 100 different optimized rotaxane co-conformers, all of which started from the same initial crown ring structure. Figure 2 shows the initial crown ring structure (cylinders rendering) and four final structures (wires rendering) selected to show the range of final structures produced. These final crown ring structures include structures that have *qualitatively different* chirality.

As further evidence of the flexibility of the crown ring, we note that in the above sample of ring structures, the RMS displacement of the atoms during optimization is always in the range 1.2−2.0 Å. The RMS maximum displacement over the set of ring structures is 2.8 Å. These values are in excess of typical bond lengths, indicating considerable structural distortion during optimization.

To quantify the production of enantiomers of both "left" and "right" chirality, we recognize that the backbone conformation is set by the dihedral angles and apply the sum of all 24 dihedral angles along the ring backbone as an index of chirality, *D*. We computed *D* for the crown ether ring components extracted from 100 different optimized rotaxane co-conformers, all of which started from the same initial crown ring structure. The results are shown in Figure 3a. Note that the *D* values of the optimized structures tend to cluster near multiples of 360 degrees, and both positive and negative values are produced. Structures with equal but opposite values of *D* have ring backbones that are mirror images of each other, i.e., opposite chirality. (Technically, this statement is rigorous only when all dihedral angles are exactly equal, but opposite in sign.) The histogram along the right vertical axis shows that pairs of enantiomers are produced with near equal probability. Very similar results were found for the second starting ring structure as shown in Figure 3b.

It is important to note that the production of rings of opposite chirality from a single starting structure does not necessarily generalize to other rotaxanes. Large crown ethers are floppy,[27,28] but other ring structures used as rotaxane components, in particular cyclodextrins, cannot readily undergo such interconversion and the procedure for generating rotaxane starting structures would require sampling both relative position and *direction of threading* of the rings upon the shaft.[29]

For all 22464 [3]rotaxane starting structures, an abbreviated geometric optimization consisting of 10 optimization steps was carried out at the AM1 level. In the language of our statistical

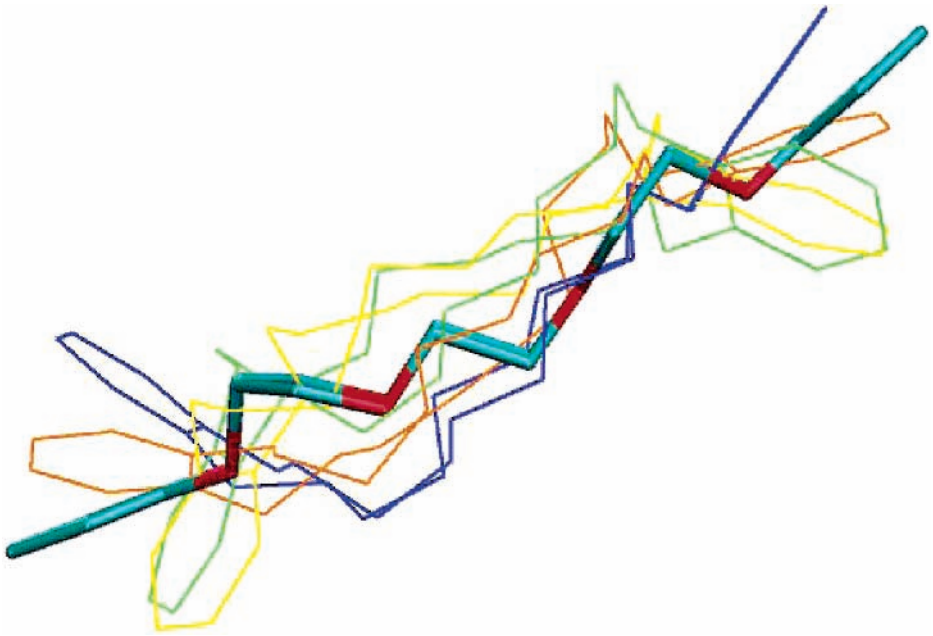

Figure 2. Initial crown ring structure (cylinders rendering) and four final structures (wires rendering) produced upon optimization of different starting structures of the [3]rotaxane showing the range of final structures produced.

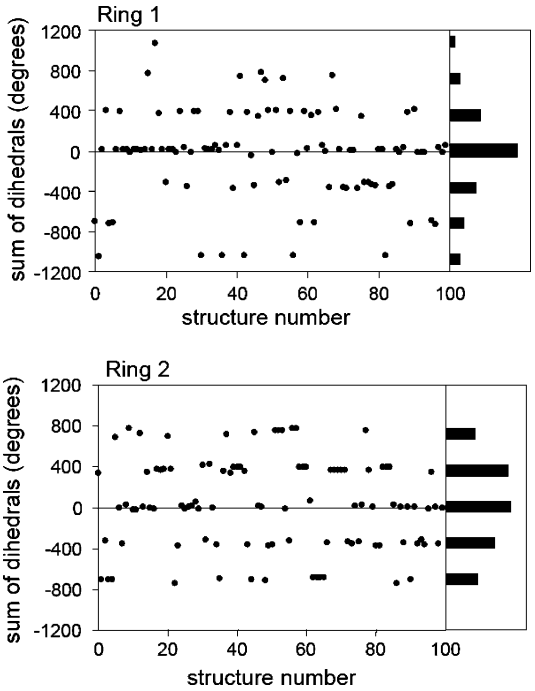

Figure 3. Sum of the 24 dihedral angles along the crown ether ring backbone for each of 100 structures produced by optimization of 100 starting structures of the [3]rotaxane, all of which contained the same starting structure for the ring. Note that the values tend to cluster near multiples of 360 degrees. The histogram along the right vertical axis shows the frequency for each group. Results are shown for each of the two starting ring structures (**3a** and **3b**).

procedure, this approximation brings the starting structures to approximate co-conformations as defined by the AM1 Hamiltonian. Next, full geometrical optimizations for the 100 lowest-energy co-conformations were performed at the same level, to confirm the structure−energy profile and to obtain some fine structural details.

2.5. Structural Assignment. Systematic analysis of the co-conformations was performed for the entire set of structures, (those optimized for 10 steps) to draw inferences about the structure−energy relationship. For each structure, the binding site of each ring component was denoted in terms of the shaft segment that pierces through the ring. In practice, this is realized by finding the segment for which the distance from its midpoint to the geometrical centroid of the corresponding ring is a shortest. Next, each structure was assigned as either *adjacent* (*prox*) or *separated* (*dist*), depending on the relative location of the two ring components on the shaft backbone. Given that the three ideal potential binding sites on the shaft are on segments 3, 7, and 11 respectively, the ideal distance between the two ring components is four segments (=7−3) in *prox* conformations, and it is eight segments (=11−3) in *dist* conformations. After abbreviated optimization, the segments were numbered so that the sum of the ring positions has the smallest possible value and the binding sites of both rings were updated upon full optimization.

2.6. Computational Details. Conformational searching of the rotaxane components was carried out at the MM level, using the SCAN module in the Tinker software,[24,25,30−33] where the following modes and parameters are used: (1) automatic selection of torsional angles; (2) setting the number of searching directions for local search as 50; (3) 50.0 kcal mol^{-1} energy threshold for local minima; (4) 0.0001 kcal mol^{-1} A^{-1} rms gradient per atom; (5) setting the time limit for each search with unique starting geometry as 1 h. As discussed at length elsewhere,[24,25] the MM3 2000[34−38] force field was selected for the conformational searching because it has been reported to be capable of predicting structural properties of a wide variety of molecular systems with reasonable accuracy,[36−38] with discrepancies between the MM3 predicted structures and crystal structures generally within the range of experimental uncertainties.[39] Support for the choice of the MM3 force field also comes from refs 35, 40, and 41, where the MM3 was reported to be capable of predicting the low energy conformations of crown ethers, species related to the ring components of the rotaxane considered here. It reportedly works well both in the reproduction of structure[42,43] and conformational energy diferences.[40,41]

Abbreviated (10-step) optimizations for all 22464 starting structures and the full geometrical optimizations for the subset of 100 lowest energy co-conformations were performed at the semiempirical (AM1) level. All semiempirical calculations (single point and geometry optimizations) were performed with the GAMESS program.[39] Previous success in treating inclusion phenomena with semiempirical methods[44−46] provides support to this approximation. Semiempirical methods, like ab initio methods, are based on an inherently quantum-mechanical description of the electronic structure, which is essential for modeling different charge states, but unlike ab initio methods are sufficiently efficient for practical calculations on systems of this size. AM1 has been found to be qualitatively acceptable for intermolecular hydrogen bonding,[47] the dominant interaction between components here. Its performance is reported to be especially good if comparisons are to be done within a class of compounds, wherein *relative* hydrogen bond strengths are predicted with high accuracy.[47] Additional support for the choice of AM1 to identify conformational preferences in the present rotaxane system comes from ref 48, wherein AM1 calculations are reported for >60 conjugated organic molecules, many with structural subunits similar to those of many known rotaxanes. It was found that within the chosen set of compounds, conformational preferences were, "quite satisfactorily calculated," an assertion reinforced by work of Dávila and Caldas.[49] Our calculations neglect dispersive forces, but these are not expected to be sufficiently large to influence any of the conclusions drawn here. For computational expediency, we have thus far neglected solvents (or supporting surfaces). This approximation has been demonstrated to work very well for the ammonium/crown ether interaction chemistry active in the present system,[24,50] as was also reported previously by Ricketts et al.[51] Finally we note that the functionality of interlocked molecule systems is embodied in their gross structural features, which should be captured accurately even at the semiempirical level of theory.

We have observed that our approach of multiple sampling with abbreviated optimization requires 18−55 times less compute time than full optimization of all structures. (On the basis of a representative subset we estimate the average gain to be ×38.)

3. Results and Discussion

3.1. Results from Abbreviated (10-Step) Geometrical Optimization. We desire to produce a structural-energy profile for the [3]rotaxane that illustrates the structural and binding preference of the system, including the folding of the shaft and the binding preferences of the two rings on the shaft. Toward this end, 22 464 starting structures were constructed here from MM optimized components and subjected to abbreviated structural optimization as discussed in section 2. Systematic analyses of the results were performed to correlate some structural features to energy.

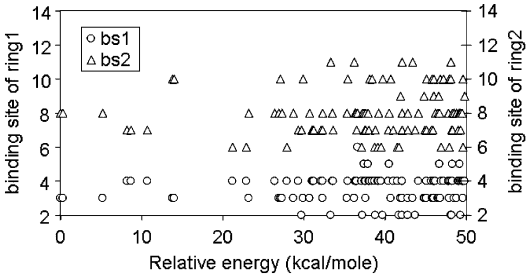

Figure 4. Binding sites of the two ring components vs energy of the [3]rotaxane (referenced to the lowest energy co-conformation found) based on abbreviated geometrical optimizations. Note that there are two points per isomer.

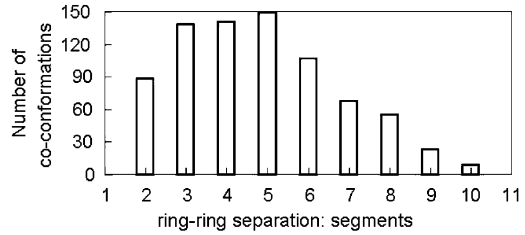

Figure 5. Histogram showing the number of conformations vs the ring−ring distance in segments based on abbreviated geometric optimizations.

3.1.1. Co-Conformational Preference: *prox* or *dist.* Analysis of the binding sites of the two ring components on the shaft reveals the binding preference of the [3]rotaxane. Figure 4 presents the binding situation of both rings relative to the energy for each co-conformation, where all co-conformations within 50.0 kcal/mol of the lowest energy co-conformation found were considered. Apparently, the lowest energy unique co-conformations (those below 10.0 kcal/mol) have the two rings binding at positions 3, 8 or 4, 7. Considering that the three ideal potential $-NH_2^+$-based binding sites are positions 3, 7, and 11 respectively, with the two rings positioned four and eight segments away in the adjacent and separated situations respectively, we deduce that the lowest energy conformations prefer to have the two ring components binding adjacent to each other instead of binding separately at the two ends. Figure 5 shows a histogram of the number of conformations vs the ring−ring separation given in segments. It suggests that most structures have two rings binding at positions 3, 4, or 5 segments apart, and these situations may be identified as *prox* structures. On the basis of the above two cases, we conclude that *prox* structures are preferred in the low energy regime over *dist* structures. This result is fully consistent with the experimental determination that *prox* structures are more enthalpically stable.[1]

3.1.2. Radius of Gyration. To further identify the structural features of the ensemble of structures we have studied the radius of gyration for the shaft in all structures with energy <50 kcal/mol. This set contains 78 *prox* and 27 *dist* co-conformations. These subsets were analyzed separately. Figure 6 shows the probability distribution vs radius of gyration (μ) for the two sets of structures: *dist* structures show an averaged μ value of 13.16 ± 0.43 amu Å^2 and *prox* structures have $\mu = 12.98 \pm 0.35$ amu Å^2.

While Figure 6 shows some slight difference in the distributions of μ between *dist* and *prox* samples, we cannot say with high confidence that there is a statistically significant difference in the means. Subjecting the use of two sets of data to statistical analysis we obtained a *t*-test value (t_{cal}) of 1.89. At confidence level of 95% for a total 105 (78 + 27) data points, the tabulated *t* value (t_{tab}) is 1.98, (which is > t_{cal}) indicating that the two

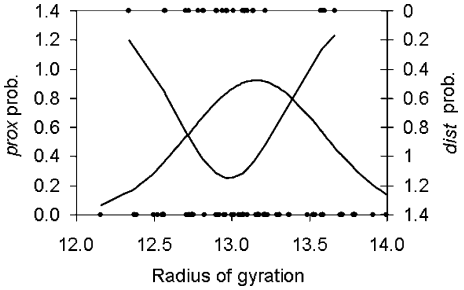

Figure 6. Best-fit normal distribution vs radius of gyration (μ) in amu Å^2, for *dist* (left vertical axis) and *prox* (right vertical axis) structures. Actual computed radii of gyration are depicted on corresponding abscissae.

distributions are not significantly different at the 95% confidence level. This result is in marked contrast to what was observed for the [2]rotaxane system studied in ref 24, where displacement of the ring upon co-conformational isomerization opened up new possibilities for inter-component hydrogen bonding leading to coiling of the shaft.

3.2. Full Geometrical Optimization. As discussed above, analysis of the co-conformations from abbreviated geometrical optimization reveals a structural profile that is qualitatively consistent with experiments.[1] To obtain a more detailed understanding of the structure−energy correlation and estimate the activation energy for switching between different co-conformations, full geometry optimizations were carried out for the 100 lowest energy co-conformations found.

3.2.1. Local Conformational Change. We have shown that a qualitatively correct structure−energy profile may be extracted from a set of approximate co-conformations. We now show that the effect of full optimization, for both approximate *prox* and *dist* initial geometries, is to slide the rings along the shaft and produce more exact *prox* and *dist* co-conformations. Shown in Figure 7 are the two low-energy approximate *prox* co-conformations (**7a** and **7b**) and the lowest-energy *dist* co-confirmation (**7c**). It may be seen that the optimizations bring the rings into the exact *prox* (3, 7) positions (**7a**) and (**7b**), or exact *dist* (3, 11) (**7c**) position. After full optimization, the lowest energy *prox* co-conformation is favored by 5.61 kcal/mol over the lowest energy *dist* co-conformation. (While qualitatively correct, this number is likely to be significantly exaggerated due to the neglect of solvent and counterions.[52])

3.2.2. Structure and Binding. On the basis of the set of fully optimized co-conformations, in the low energy regime, all structures take-on co-conformations with the two rings binding on adjacent (*prox*) positions rather than separated (*dist*) ones. As shown in Figure 8, among the 100 structures chosen for full optimization, a majority of them (a total of 51) in all energy ranges, and all of them (in total, 16) in the low energy region (those within 5.43 kcal/mol of the lowest energy co-conformation found) have the two ring components binding at positions (3, 7), which represents the ideal *prox* co-conformation. (Note, however, that the optimizations do not necessarily start with an exact *prox* co-conformation.)

The binding situation is further illustrated in Figure 9, which is based on the results of the 100 fully optimized co-conformations. Again we see clear evidence that *prox*-conformations are preferred over the *dist* ones in low energy structures.

3.2.3. Origin of Co-Conformational Preference. On the basis of the above discussion, *prox* co-conformations are favored over *dist* ones. To identify the origin of this preference, we have carried out calculations of the inter-component interactions. The

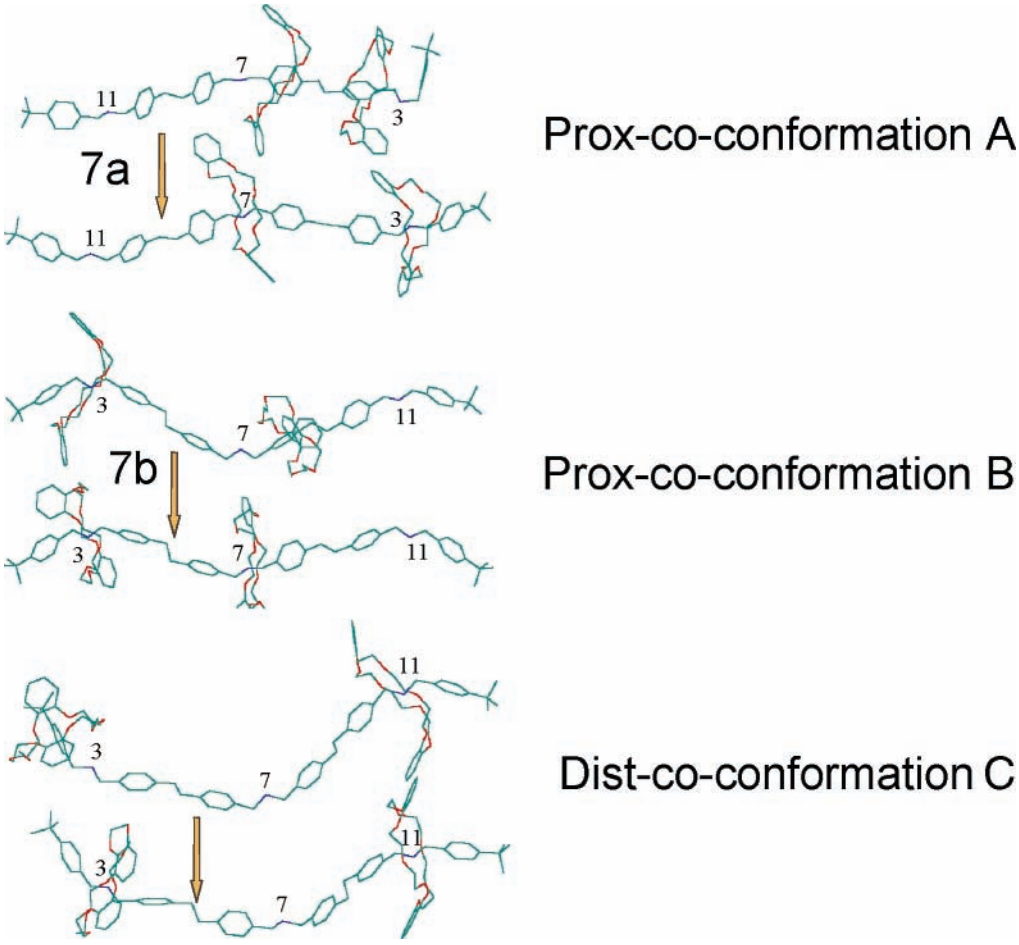

Figure 7. Local conformational change by the full optimization. Shown are the two lowest-energy *prox* co-conformations and the lowest-energy *dist* co-conformation.

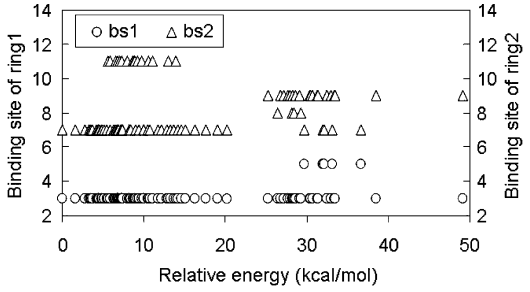

Figure 8. Binding sites of two ring components vs energy of the [3]-rotaxane (referenced to the lowest energy co-conformation found) based on full geometrical optimizations.

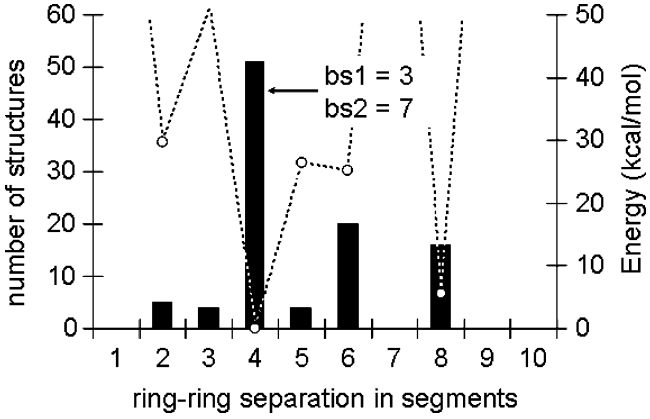

Figure 9. Histogram depicting the number of structures vs the distance between the two ring components (in segments) based on full geometrical optimizations. The Boltzmann-averaged relative energies (right-hand vertical axis) are depicted by open circles, connected by dashed lines to guide the eye. Note that the minimum energies correspond to structures with ring−ring distances of four or eight segments, i.e., *prox* and *dist* structures. 95% of the structures with a ring−ring distance of four segments have the two rings binding at positions 3 and 7, the exact locations of the two adjacent amide groups representing the two ideal binding sites.

lowest-energy fully optimized *dist* and *prox* co-conformations were used, and the ring−ring and ring−shaft interactions were analyzed for the three sub-components. Single-point total energies for the [3]rotaxane complexes and their isolated components were calculated. The results are shown in Table 2.

This analysis shows that the ring−ring interaction is very small in both *dist* and *prox* co-conformations. Not surprisingly it is weaker in the *dist* case where the separation of the rings is greater. (See top section of Table 2.) As presented in the middle section of Table 2, *prox* co-conformers have stronger ring−shaft binding and are therefore lower in energy than *dist* co-conformers, although the *prox* subcomponents taken individually are slightly higher in total energy than the *dist* subcomponents. This is an important result because it shows that the lowest energy complex is not necessarily constructed from the lowest energy structures of the sub-components. In constructing the full complex, therefore, it is essential to consider subcomponent structures over a range of energies, as has been done here.

As a further test, we computed single point energies for a pair of [2]rotaxanes with a single ring on site 3 and 7, respectively. (See the bottom section of Table 2.) Since the terminal binding sites are chemically distinct from the central

TABLE 2: Energies of Individual Components and Intercomponent Interactions

system	energy (hartree) prox (3,7)	dist (3,11)	[2]rotaxane[a]
ring1	−223.25560	−223.26271	
ring2	−223.25522	−223.25660	
sum of the two ring components	−446.51083	−446.51932	
ring1-ring2 complex	−446.51054	−446.51928	
interaction in ring1−ring2 complex	**0.00028**	**4.E−05**	
shaft	−310.51746	−310.51424	
summation of the three subcomponent	−757.02829	−757.03356	
shaft-ring1-ring2 complex	−757.19372	−757.184331	
interaction in shaft−ring1−ring2 complex	**−0.16543**	**−0.15076**	
ring (pos3)-shaft complex			−533.85425
ring (pos7)-shaft complex			−533.85833
interaction in ring (pos3)−shaft complex			**−0.08119**
interaction in ring (pos7)−shaft complex			**−0.08565**

[a] Each [2]rotaxane is formed by deleting one ring from the full [3]rotaxane complex. pos3 denotes a co-conformation with one ring binding at position 3, and pos7 denotes a co-conformation with one ring binding at position 7

binding site, the strength of ring binding may differ in these two cases and in fact it is found that the ring−shaft interaction is stronger with the ring on site 7 (−0.08565 hartree) than on site 3 (−0.08119 hartree). Given that the two rings are essentially noninteracting, a [3]rotaxane with binding at positions 3 and 7 is lower in energy than a [3]rotaxane with binding at positions 3 and 11. Therefore, we conclude that it is the ring−shaft inter-component interactions that decide the co-conformational preference of the [3]rotaxane. In other words, the preference is really for having a ring at position 7, rather than for having adjacent rings. This result has important implications for the construction of multiple rotaxanes based on the ammonium/crown ether interaction chemistry active of the present system but containing longer shafts with more ammonium stations; co-conformational selectivity will be determined by ring−shaft interactions, not a "*prox* preference".

4. Conclusions

A modeling procedure based on large-scale multiple sampling and statistical analysis of a large set of co-conformations, which has shown previous success for the modeling of switchable rotaxane and catenane systems, was applied here to an experimentally realized [3]rotaxane to investigate its multiple stability. The results of this investigation are summarized as follows:

(1) Statistical analysis of the structure−energy profile generated from a large set of structures that have been subjected to abbreviated structural optimization, shows that the molecule prefers to take-on the *prox* co-conformations rather than the *dist* co-conformations, in agreement with experimental observations[1].

(2) Full geometric optimization of a subset of the approximate co-conformations confirms the above result. As is a basic assumption of the multiple sampling and statistical analysis procedure, full structural optimization has the effect of bringing that structures closer to "true" *dist* or *prox* co-conformations, but does not qualitatively change the structure−energy profile.

(3) The *t*-test analysis reveals that co-conformational preference has no statistically significant correlation to backbone coiling (at the 95% confidence level), an interesting result given the obvious necessity to provide sufficient space to accommodate the two bulky rings components.

(4) Ring−ring interactions are found to be very small, and ring−shaft inter-component interactions decide the co-conformational preference, a result with important implications for the construction of larger multiple rotaxanes based on the ammonium/crown ether interaction chemistry.

The study reported here represents the application of the multiple sampling and statistical analysis procedure to an interlocked molecule of greater size and topological complexity than any previously treated. Given that the functionality of molecular nano devices is embodied in their gross structural features, the ability to reliably reproduce these gross features suggest that the modeling technique may be useful to accelerate iterative molecular design and refinement for targeted mechanical properties.

Acknowledgment. This work was funded by NSF Awards CHE0449595 and BES0102848 and by Dupont Corp. in the form of a Dupont Young Professor award to K.S.

References and Notes

(1) Chiu, S. H.; Rowan, S. L.; Cantrill, S. J.; Stoddart, J. F.; White, A. J. P.; Williams, D. L. *Chem.−Eur. J.* **2002**, *8*, 5170.

(2) Liu, J.; Gomez-Kaifer, M.; Kaifer, A. E. *Mol. Machines Motors* **2001**, *99*, 141.

(3) Pease, A. R.; Jeppesen, J. O.; Stoddart, J. F.; Luo, Y.; Collier, C. P.; Heath, J. R. *Acc. Chem. Res.* **2001**, *34*, 433.

(4) Pease, A. R.; Stoddart, J. F. *Mol. Machines Motors* **2001**, *99*, 189.

(5) Schalley, C. A.; Beizai, K.; Vogtle, F. *Acc. Chem. Res.* **2001**, *34*, 465.

(6) Anelli, P. L.; Asakawa, M.; Ashton, P. R.; Bissell, R. A.; Clavier, G.; Gorski, R.; Kaifer, A. E.; Langford, S. J.; Mattersteig, G.; Menzer, S.; Philp, D.; Slawin, A. M. Z.; Spencer, N.; Stoddart, J. F.; Tolley, M. S.; Williams, D. J. *Chem.−Eur. J.* **1997**, *3*, 1113.

(7) Ashton, P. R.; Huff, J.; Menzer, S.; Parsons, I. W.; Preece, J. A.; Stoddart, J. F.; Tolley, M. S.; White, A. J. P.; Williams, D. J. *Chem.−Eur. J.* **1996**, *2*, 31.

(8) Amabilino, D. B.; Stoddart, J. F. *Chem. Rev.* **1995**, *95*, 2725.

(9) Ballardini, R.; Balzani, V.; Credi, A.; Gandolfi, M. T.; Venturi, M. *Mol. Machines Motors* **2001**, *99*, 163.

(10) Chen, H. L. *Chinese, J. Inorg. Chem.* **2001**, *17*, 1.

(11) Breault, G. A.; Hunter, C. A.; Mayers, P. C. *Tetrahedron* **1999**, *55*, 5265.

(12) Claessens, C. G.; Stoddart, J. F. *J. Phys. Org. Chem.* **1997**, *10*, 254.

(13) Jager, R.; Vogtle, F. *Angew. Chem., Int. Ed. Engl.* **1997**, *36*, 930.

(14) Belohradsky, M.; Raymo, F. M.; Stoddart, J. F. *Collect. Czech. Chem. Commun.* **1997**, *62*, 527.

(15) Raymo, F. M.; Stoddart, J. F. *Curr. Opin. Colloid Interface Sci.* **1996**, *1*, 116.

(16) Pasini, D.; Raymo, F. M.; Stoddart, J. F. *Gazz. Chim. Ital.* **1995**, *125*, 431.

(17) Amabilino, D. B.; Stoddart, J. F.; Williams, D. J. *Chem. Mater.* **1994**, *6*, 1159.

(18) Reuter, C.; Schmieder, R.; Vogtle, F. *Pure Appl. Chem.* **2000**, *72*, 2233.

(19) Chiu, S. H.; Elizarov, A. M.; Glink, P. T.; Stoddart, J. F. *Org. Lett.* **2002**, *4*, 3561.

(20) Leigh, D. A.; Troisi, A.; Zerbetto, F. *Chem.−Eur. J.* **2001**, *7*, 1450.

(21) Deleuze, M. S.; Leigh, D. A.; Zerbetto, F. *J. Am. Chem. Soc.* **1999**, *121*, 2364.

(22) Leigh, D. A.; Murphy, A.; Smart, J. P.; Deleuze, M. S.; Zerbetto, F. *J. Am. Chem. Soc.* **1998**, *120*, 6458.

(23) Raymo, F. M.; Houk, K. N.; Stoddart, J. F. *J. Org. Chem.* **1998**, *63*, 6523.
(24) Zheng, X.; Sohlberg, K. *J. Phys. Chem. A.* **2003**, *107*, 1207.
(25) Zheng, X.; Sohlberg, K. *Phys. Chem. Chem. Phys.* **2004**, *6*, 809.
(26) Dewar, M. J. S.; Zoebisch, E. G.; Healy, E. F.; Stewart, J. J. P. *J. Am. Chem. Soc.* **1985**, *107*, 3902.
(27) Wipff, G.; Weiner, P.; Kollman, P. *J. Am. Chem. Soc.* **1982**, *104*, 3249.
(28) Glendening, E. D.; Feller, D.; Thompson, M. A. *J. Am. Chem. Soc.* **1994**, *116*, 10657.
(29) Schalley, C. A.; Beizai, K.; Vogtle, F. *Acc. Chem. Res.* **2001**, *34*, 465.
(30) Dudek, M. J.; Ponder, J. W. *J. Comput. Chem.* **1995**, *16*, 791.
(31) Kundrot, C. E.; Ponder, J. W.; Richards, F. M. *J. Comput. Chem.* **1991**, *12*, 402.
(32) Ponder, J. W. *Software Tools for Molecular Design.* Version 3.9. Copyright 1990−2001. http://dasher.wustl.edu/tinker/.
(33) Ponder, J. W. *J. Comput. Chem.* **1987**, *8*, 1016.
(34) Allinger, N. L.; Durkin, K. A. *J. Comput. Chem.* **2000**, *21*, 1229.
(35) Hay, B. P.; Yang, L. R.; Lii, J. H.; Allinger, N. L. *J. Mol. Struct. (THEOCHEM)* **1998**, *428*, 203.
(36) Allinger, N. L.; Yuh, Y. H.; Lii, J. H. *J. Am. Chem. Soc.* **1989**, *111*, 8551.
(37) Lii, J. H.; Allinger, N. L. *J. Am. Chem. Soc.* **1989**, *111*, 8566.
(38) Lii, J. H.; Allinger, N. L. *J. Am. Chem. Soc.* **1989**, *111*, 8576.
(39) Schmidt, M. W.; Baldridge, K. K.; Boatz, J. A.; Elbert, S. T.; Gordon, M. S.; Jensen, J. H.; Koseki, S.; Matsunaga, N.; Nguyen, K. A.; Su, S. J.; Windus, T. L.; Dupuis, M.; Montgomery, J. A. *J. Comput. Chem.* **1993**, *14*, 1347.
(40) Paulsen, M. D.; Rustad, J. R.; Hay, B. P. *J. Mol. Struct. (THEOCHEM)* **1997**, *397*, 1.
(41) Hay, B. P.; Rustad, J. R.; Zipperer, J. P.; Wester, D. W. *J. Mol. Struct. (THEOCHEM)* **1995**, *337*, 39.
(42) Hay, B. P.; Yang, L. R.; Zhang, D. L.; Rustad, J. R.; Wasserman, E. *J. Mol. Struct. (THEOCHEM)* **1997**, *417*, 19.
(43) Hay, B. P.; Rustad, J. R. *J. Am. Chem. Soc.* **1994**, *116*, 6316.
(44) Liu, L.; Li, X. S.; Song, K. S.; Guo, Q. X. *J. Mol. Struct. (THEOCHEM*) **2000**, *531*, 127.
(45) Sohlberg, K.; Sumpter, B. G.; Noid, D. W. *J. Mol. Struct. (THEOCHEM)* **1999**, *491*, 281.
(46) Sohlberg, K.; Tarbet, B. J. *J. Incl. Phenom. Mol. Recogn. Chem.* **1995**, *23*, 203.
(47) Buemi, G.; Zuccarello, F.; Raudino, A. *J. Mol. Struct. (THEOCHEM)* **1988**, *164*, 379.
(48) Fabian, W. M. F. *J. Comput. Chem.* **1988**, *9*, 369.
(49) Davila, L. Y. A.; Caldas, M. J. *J. Comput. Chem.* **2002**, *23*, 1135.
(50) Frankfort, L.; Sohlberg, K. *J. Mol. Struct. (THEOCHEM)* **2003**, *621*, 253.
(51) Ricketts, H. G.; Stoddart, J. F.; Hann, M. M. A simple approach to modellinig supramolecular complexes and mechanically interlocked molecules. In *Computational Approaches in Supramolecular Chemistry*; Wipff, G., Ed.; Series C: Mathematical and Physical Science 426; Kluwer Academic Publishers: Netherlands, 1994; p 377.
(52) Grabuleda, X.; Ivanov, P.; Jaime, C. *J. Org. Chem.* **2003**, *68*, 1539.